ORIGINAL

P. Das · M. A. Islam⬚ · S. Somadder · M. A. Hasib

# Analytical and numerical solutions of pressurized thick-walled FGM spheres

Abstract The elastic analysis of thick-walled spheres made of functionally graded materials (FGMs) is considered to be one of the most important areas in many engineering designs. This paper presents the stresses and displacement fields in an FGM thick-walled sphere under constant interior and exterior pressure. The investigation was carried out using analytical and numerical methods. Exact and finite element (FE) models of the pressurized spherical vessel were created, assuming and implementing continuous changing of Young modulus along the radial direction. It is considered that the elastic modulus of the FGMs varies with thickness according to the nonlinear generalized formula. For a pressurized FGM sphere, the analytical solutions for displacement and stress distribution were developed and demonstrated in the radial direction. Finally, the analytical results are compared to the results from the FE analysis.

1 Introduction

Functionally graded materials (FGMs) are a special type of heterogeneous materials whose material properties continuously change over the domain. These materials are made up of two or more separate material phases, the volume fractions of which are constantly varying when spatial factors change. Heterogeneous hybrid composites are FGMs that have a gradient compositional variability of elements from one surface to the other, resulting in constantly evolving material characteristics. In recent few years, several studies regarding mechanical structures composed of FG materials have been carried out [1–8]. Tutuncu and Ozturk [9] found closed-form solutions for cylindrical and spherical vessels with varying elastic characteristics following a simple power law over the domain, resulting in simple Cauchy–Euler equations with readily available solutions. You et al. [10] investigated the elastic properties of an internally pressured thick-walled sphere made of FGMs. There are two types of pressure vessels: one has two homogenous layers along the vessel's inner and outer surfaces, and the other has a functionally graded layer in the center; the other has just functionally graded material. The thermo-mechanical stresses in an FGM hollow thick sphere were investigated by Eslami et al. [11]. In their article, except for Poisson's ratio, the material characteristics were supposed to vary over the radius according to a power-law function. The temperature profile, radial displacement, radial stress, and hoop stress as a function of radial direction are obtained by solving the heat conduction equation and the Navier equation analytically. Under asymmetric thermo-mechanical loads, Poultangari et al. [12] studied the various thermo-mechanical stresses in a thick hollow FGM sphere. Chen and Lin [13] performed elastic studies for thick cylindrical and spherical FG pressure pipes using an exponential change of material stiffness. Tutuncu and Temel [14] developed a novel methodology to stress analysis of pressurized hollow thick FGM cylinders, disks,

P. Das · M. A. Islam (✉) · S. Somadder · M. A. Hasib
Department of Mechanical Engineering, Khulna University of Engineering & Technology, Khulna 9203, Bangladesh
e-mail: md.islam@me.kuet.ac.bd
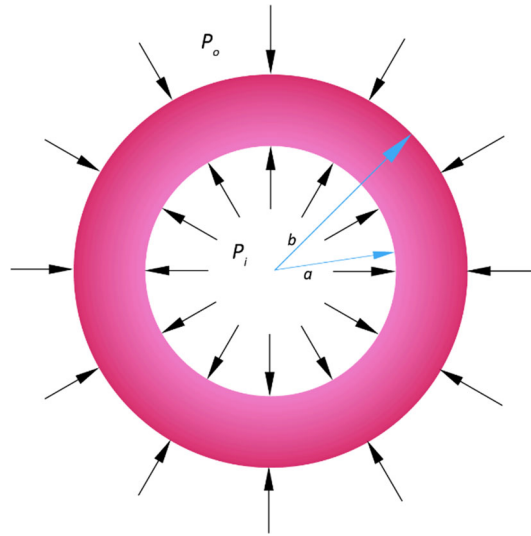
Fig. 1 Thick-Walled FGM sphere

and spheres using the complementary function method. Borisov [15] investigates deformations and stresses inside multilayered thick-walled spheres. Sadeghian and Toussi [16] investigated the thermo-elasto-plastic behavior of an FGM spherical vessel under thermo-mechanical loads. They evaluated power-law variation for material properties, including both mechanical and thermal characteristics, in this research, whereas the Poisson ratio was assumed to be constant throughout the thickness. Using an exponential and parabolic law in material characteristics, Nejad et al. and Karimi et al. developed analytical solutions for FGM thick-walled spherical shells exposed to interior and exterior pressure [17, 18]. Also, the characteristics of an FGM-coated spherical pressure vessel that vary material properties linearly and exponentially are investigated by Atashipour et al. [19].

So far in the literature, the only analytical solutions that are available for the elastic field in spheres are when the Young modulus is defined by the power law and exponential law. There is little to no work available in the literature that addresses the Young modulus in the general formula without power law and exponential law. A more generic expression for the spatial variation of the Young modulus of material given in the literature [20] was adopted in this research. In the presence of interior and exterior pressures, we investigated the stress fields in a thick spherical pressure vessel in FGMs. Here, the Poisson ratio is assumed to be constant, and material stiffness is given by a nonlinear generalized formula with four parameters (see Eq. 4). The equilibrium equation is converted into a linear homogeneous differential equation, which is solved analytically.

The pressurized vessel was also modeled using finite element analysis (FEA), where a FE code (USDFLD) was used to implement the continuous variation of material stiffness along with the thickness. Following that, we contrasted the exact and FE results.

2 Mathematical model description

The model is considered a hollow FGM sphere whose internal and external radius a, respectively. P_i and P_o are uniform pressure loads, both internally and externally. The FGM materials are considered to be linearly elastic, and the Young modulus follows a nonlinear function depending on the radial axis only, where the Poisson ratio is considered to be invariant.

A schematic diagram of the FGM sphere is given in Fig. 1.

For convenience, axisymmetric boundary conditions (BC) are necessitated for this case requires assuming a spherical coordinate (r, θ, ϕ).

Since the load is axisymmetric and uniform, the displacement and stress fields are identical in θ and ϕ direction. The stress and strain fields in the theory of plane elasticity can be stated as follows:

$$\sigma_{ij} = \sigma_{ij}(r) \ , \ \varepsilon_{ij} = \varepsilon_{ij}(r)$$
$$\mathbf{u} = \mathbf{u}(r) \, , \mathbf{u} = u \, \mathbf{e_i}$$

where **u** is the displacement vector.

The material parameter is the function of r as it is graded along the radial direction. Assume u_r is radial displacement field since the problem is axisymmetric.

Kinematic relations are given:

$$\begin{cases} \varepsilon_{rr} = \dfrac{\mathrm{d}u_r}{\mathrm{d}r} \\ \varepsilon_{\theta\theta} = \varepsilon_{\phi\phi} = \dfrac{u_r}{r} \\ \varepsilon_{r\phi} = \varepsilon_{r\theta} = \varepsilon_{\theta\phi} = 0 \ (\text{No shear deformation}) \end{cases} \tag{1}$$

Stress–strain relationship from kinematic Eq. (1) can be written:

$$\begin{Bmatrix} \sigma_{rr} \\ \sigma_{\theta\theta} \end{Bmatrix} = G(E(r), \nu) \begin{bmatrix} (1-\nu) & 2\nu \\ \nu & 1 \end{bmatrix} \begin{Bmatrix} \dfrac{\mathrm{d}u_r}{\mathrm{d}r} \\ \dfrac{u_r}{r} \end{Bmatrix} \tag{2}$$

where $G(E(r), \nu) = \frac{E(r)}{(1+\nu)(1-2\nu)}$

Due to the absence of gravitational forces from the equilibrium, equation of motion in a spherical coordinate system can be written as follows:

$$\frac{\mathrm{d}\sigma_{rr}}{\mathrm{d}r} + \frac{2}{r}(\sigma_{rr} - \sigma_{\theta\theta}) = 0 \tag{3}$$

where σ_{rr} and $\sigma_{\theta\theta}$ are the radial and hoop stress, respectively.

It is necessary to be familiar with the functional relations of the mechanical properties in order to derive the equilibrium equation for the FGM sphere expressed in terms of the radial displacement component. A special formula of material stiffness throughout the thickness is addressed to determine the effect of inhomogeneity [20]:

$$E(r) = E_i \left(\frac{r}{a}\right)^m e^{\gamma\{(\frac{r}{a})^s - 1\}} \tag{4}$$

Substituting the stress–strain relationship in Eq. (2) into the equation of motion in Eq. (3), Navier's equation can be expressed as follows:

$$r^2 \frac{\mathrm{d}^2 u_r}{\mathrm{d}r^2} + r\left(2 + \frac{r}{E(r)}\frac{\mathrm{d}E(r)}{\mathrm{d}r}\right)\frac{\mathrm{d}u_r}{\mathrm{d}r} - 2\left(1 - \nu^* \frac{r}{E(r)}\frac{\mathrm{d}E(r)}{\mathrm{d}r}\right)u_r = 0 \tag{5}$$

where $\nu^* = \frac{\nu}{1-\nu}$.

Then, substituting Eq. (4) into Eq. (5), the differential equation is obtained as:

$$r^2 \frac{\mathrm{d}^2 u_r}{\mathrm{d}r^2} + r\frac{\mathrm{d}u_r}{\mathrm{d}r}\left\{s\gamma\left(\frac{r}{a}\right)^s + m + 2\right\} + 2\left[\nu^* m + s\gamma\left(\frac{r}{a}\right)^s - 1\right]u_r = 0 \tag{6}$$

As solid is incompressible and $\nu < \frac{1}{2}$ [20], $E(r)$ can be written as $E(r) \propto r^m$ so that $\frac{r}{E(r)}\frac{\mathrm{d}E(r)}{\mathrm{d}r} = m$. Equation (5) then reduces to the Cauchy–Euler equation. The indicial equation from the above equation can be written as:

$$\xi(\xi - 1) + (2 + m)\xi - 2(1 - m\nu^*) = 0 \tag{7}$$

where ξ is the real root of the indicial equation. The two distinct roots are:

$$\xi_1 = -\frac{1}{2}\left\{(m+1) - \sqrt{m^2 + 2m(1 - 4\nu^*) + 9}\right\}$$

$$\xi_2 = -\frac{1}{2}\left\{(m+1) + \sqrt{m^2 + 2m(1 - 4\nu^*) + 9}\right\}$$

Using a new variable $x = \gamma\left(\frac{r}{a}\right)^s$ and Eq. (7) and then applying the transformation $u(r) = r^\xi y(x)$, the result of Eq. (6) is:

$$x\frac{\mathrm{d}^2 y(x)}{\mathrm{d}x} + (b + x)\frac{\mathrm{d}y(x)}{\mathrm{d}x} + ay(x) = 0 \tag{8}$$

where, $b = \dfrac{s + 2\xi + m + 1}{s}$

$a = \dfrac{2v^* + \xi}{s}$

Equation (8) is a confluent hyper geometric differential equation (Kummer's function). The solution is written in the following form [21, 22]:

$$y(x) = A\, e^{-x} M(b_1 - a_1, b_1, x) + B\, e^{-x} M(b_2 - a_2, b_2, x) \tag{9}$$

A and B are constant that to be determined using traction boundary conditions.

$M(b_1 - a_1, b_1, x)$ is a Kummer's function.

Substituting back original variable to Eq. (9), it can be written as:

$$u(r) = A\, r^{\xi_1} e^{-\gamma\left(\frac{r}{a}\right)^s} M\left(\alpha_1, b_1, \gamma\left(\frac{r}{a}\right)^s\right) + B\, r^{\xi_2} e^{-\gamma\left(\frac{r}{a}\right)^s} M\left(\alpha_2, b_2, \gamma\left(\frac{r}{a}\right)^s\right) \tag{10}$$

where, $\alpha_1 = b_1 - a_1 = \dfrac{s + 2\xi_1 + m + 1}{s} - \dfrac{2v^* + \xi_1}{s}$

$\alpha_2 = b_2 - a_2 = \dfrac{s + 2\xi_2 + m + 1}{s} - \dfrac{2v^* + \xi_2}{s}$

The Kummer's function $M\left(\alpha_1, b_1, \gamma\left(\frac{r}{a}\right)^s\right)$ can be expressed as power series:

$$M\left(\alpha_1, b_1, \gamma\left(\frac{r}{a}\right)^s\right) = 1 + \frac{\alpha_1\left\{\gamma\left(\frac{r}{a}\right)^s\right\}}{b_1} + \frac{\alpha_1(1+\alpha_1)\left\{\gamma\left(\frac{r}{a}\right)^s\right\}}{b_1(1+b_1)\,2!} + \ldots\ldots + \frac{(\alpha_1)_n\left\{\gamma\left(\frac{r}{a}\right)^s\right\}^n}{(b_1)_n n!} + \ldots\ldots$$

Here, $(\alpha_i)_k = \alpha_i(\alpha_i + 1)\ldots(\alpha_i + n - 1)$ is a Pochhammer's symbol.

The fundamental features of Kummer's function can be found in the scientific literature [22] as well as in computer programs.

The derivative form of Kummer's function can be written as:

$$\frac{dM(\alpha, b, x)}{dx} = \frac{\alpha}{b} M(\alpha + 1, b + 1, x)$$

Now, the derivative of Eq. 10 can be expressed as:

$$\begin{aligned}
\frac{du(r)}{dr} &= A\, r^{\xi_1 - 1} e^{-\gamma\left(\frac{r}{a}\right)^s}\left[a_1 s M\left(1 + \alpha_1, b_1, \gamma\left(\frac{r}{a}\right)^s\right) - \left\{\gamma s\left(\frac{r}{a}\right)^s + a_1 s - \xi_1\right\} M\left(\alpha_1, b_1, \gamma\left(\frac{r}{a}\right)^s\right)\right] \\
&+ B\, r^{\xi_2 - 1} e^{-\gamma\left(\frac{r}{a}\right)^s}\left[a_2 s M\left(1 + \alpha_2, b_2, \gamma\left(\frac{r}{a}\right)^s\right) - \left\{\gamma s\left(\frac{r}{a}\right)^s + a_2 s - \xi_2\right\} M\left(\alpha_2, b_2, \gamma\left(\frac{r}{a}\right)^s\right)\right]
\end{aligned} \tag{11}$$

The expression of radial stress and hoop stress can be calculated as:

$$\sigma_{\text{rr}} = G(E(r), v)\begin{bmatrix} A\, r^{\xi_1 - 1} e^{-\gamma\left(\frac{r}{a}\right)^s} M\left(\alpha_1, b_1, \gamma\left(\frac{r}{a}\right)^s\right)\left((1-v)\left\{-s\gamma\left(\frac{r}{a}\right)^s - \alpha_1 s + \xi_1\right\} + 2v\right) + \\ A\, r^{\xi_2 - 1} e^{-\gamma\left(\frac{r}{a}\right)^s} M\left(\alpha_2, b_2, \gamma\left(\frac{r}{a}\right)^s\right)\left((1-v)\left\{-s\gamma\left(\frac{r}{a}\right)^s - \alpha_2 s + \xi_2\right\} + 2v\right) \\ A\, r^{\xi_1 - 1} e^{-\gamma\left(\frac{r}{a}\right)^s}\alpha_1 s v\, M\left(1 + \alpha_1, b_1, \gamma\left(\frac{r}{a}\right)^s\right) + B\, r^{\xi_2 - 1} e^{-\gamma\left(\frac{r}{a}\right)^s}\alpha_2 s v\, M\left(1 + \alpha_2, b_2, \gamma\left(\frac{r}{a}\right)^s\right) \end{bmatrix} \tag{12}$$

$$\sigma_{\theta\theta/\phi\phi} = G(E(r), v)\begin{bmatrix} A\, r^{\xi_1 - 1} e^{-\gamma\left(\frac{r}{a}\right)^s} M\left(\alpha_1, b_1, \gamma\left(\frac{r}{a}\right)^s\right)\left(v\left\{-s\gamma\left(\frac{r}{a}\right)^s - \alpha_1 s + \xi_1\right\} + 1\right) + \\ A\, r^{\xi_2 - 1} e^{-\gamma\left(\frac{r}{a}\right)^s} M\left(\alpha_2, b_2, \gamma\left(\frac{r}{a}\right)^s\right)\left(v\left\{-s\gamma\left(\frac{r}{a}\right)^s - \alpha_2 s + \xi_2\right\} + 1\right) \\ A\, r^{\xi_1 - 1} e^{-\gamma\left(\frac{r}{a}\right)^s}\alpha_1 s v\, M\left(1 + \alpha_1, b_1, \gamma\left(\frac{r}{a}\right)^s\right) + B\, r^{\xi_2 - 1} e^{-\gamma\left(\frac{r}{a}\right)^s}\alpha_2 s v\, M\left(1 + \alpha_2, b_2, \gamma\left(\frac{r}{a}\right)^s\right) \end{bmatrix} \tag{13}$$

It is possible to obtain the value of A and B using the boundary conditions for the sphere under internal and external pressure as follows.

$$\begin{cases} \sigma_{\text{rr}}\,|_{r=a} = E(r)\left.\dfrac{du(r)}{dr}\right|_{r=a} = -P_i \\[2mm] \sigma_{\text{rr}}\,|_{r=b} = E(r)\left.\dfrac{du(r)}{dr}\right|_{r=b} = -P_o \end{cases} \tag{14}$$

Equation (14) leads to two linear systems of the equation where two unknowns, A and B, can be related as:

$$
-P_i = G(E(a), v) \begin{bmatrix} A\, r^{\xi_1-1}\, e^{-\gamma}\, M\,(\alpha_1, b_1, \gamma)\,((1-v)\{-s\gamma - \alpha_1 s + \xi_1\} + 2v) + \\ A\, r^{\xi_2-1}\, e^{-\gamma}\, M\,(\alpha_2, b_2, \gamma)\,((1-v)\{-s\gamma - \alpha_2 s + \xi_2\} + 2v) \\ A\, r^{\xi_1-1}\, e^{-\gamma}\alpha_1 s v\, M\,(1+\alpha_1, b_1, \gamma) + B\, r^{\xi_2-1}\, e^{-\gamma}\alpha_2 s v\, M\,(1+\alpha_2, b_2, \gamma) \end{bmatrix}
\tag{15}
$$

$$
-P_0 = G(E(b), v) \begin{bmatrix} A\, r^{\xi_1-1}\, e^{-\gamma\left(\frac{b}{a}\right)^s}\, M\left(\alpha_1, b_1, \gamma\left(\frac{b}{a}\right)^s\right)\left((1-v)\left\{-s\gamma\left(\frac{b}{a}\right)^s - \alpha_1 s + \xi_1\right\} + 2v\right) + \\ A\, r^{\xi_2-1}\, e^{-\gamma\left(\frac{b}{a}\right)^s}\, M\left(\alpha_2, b_2, \gamma\left(\frac{b}{a}\right)^s\right)\left((1-v)\left\{-s\gamma\left(\frac{b}{a}\right)^s - \alpha_2 s + \xi_2\right\} + 2v\right) \\ A\, r^{\xi_1-1}\, e^{-\gamma\left(\frac{b}{a}\right)^s}\alpha_1 s v\, M\left(1+\alpha_1, b_1, \gamma\left(\frac{b}{a}\right)^s\right) + B\, r^{\xi_2-1}\, e^{-\gamma\left(\frac{b}{a}\right)^s}\alpha_2 s v\, M\left(1+\alpha_2, b_2, \gamma\left(\frac{b}{a}\right)^s\right) \end{bmatrix}
\tag{16}
$$

Two algebraic Eqs. (15) and (16) can be used to derive the constants A and B from the boundary conditions of (14).

The Von-Misses stress can be written as:

$$
\sigma_{\text{misses}} = \frac{1}{\sqrt{2}}\sqrt{(\sigma_r - \sigma_\theta)^2 + (\sigma_\theta - \sigma_\phi)^2 + (\sigma_\phi - \sigma_r)^2}
\tag{17}
$$

3 Finite element analysis

In this problem, a standard Galerkin discretization approach of the finite element method is used to solve the differential Eq. (6). In this discretization, the size of each element is equal, and the total domain is divided into N elements; then, the equation is converted into simultaneous equations.

$$
\sum K_{ij} u_j^e = L_i^e \; ; i = 1, 2 \qquad e = 1, 2, \ldots\ldots N
\tag{18}
$$

where the value of K_{ij} and L_i^e is obtained from

$$
K_{ij} = \int_{r_e}^{r_{e+1}} \frac{d\Omega_i^e}{dr}\frac{d\Omega_j^e}{dr}dr + \int_{r_e}^{r_{e+1}} \frac{1}{r}\left\{s\gamma\left(\frac{r}{a}\right)^s + m + 2\right\}\Omega_i^e \frac{d\Omega_j^e}{d\overline{r}}dr
$$

$$
+ \int_{r_e}^{r_{e+1}} \frac{2}{r^2}\left[v^* m + s\gamma\left(\frac{r}{a}\right)^s - 1\right]\Omega_i^e\Omega_j^e d\overline{r} + \left[\Omega_i^e \frac{d\Omega_j^e}{d\overline{r}}\right]_{r_e}^{r_{e+1}}
$$

$$
L_i^e = 0
$$

where Ω_i^e is the linear interpolation/weighting function.

Equation (18) gives u_j^e values at different cylinder's nodal points, which are used to determine stresses as follows:

$$
\left\{\begin{matrix} \sigma_r \\ \sigma_\theta \end{matrix}\right\} = G(E(r), v)\begin{bmatrix} (1-v) & 2v \\ v & 1 \end{bmatrix}\left\{\begin{matrix} \sum\limits_{j=1}^{2} u_j^e \frac{d\Omega_j^e}{d\overline{r}} \\ \sum\limits_{j=1}^{2} \frac{u_j^e\Omega_j^e}{\overline{r}} \end{matrix}\right\}
$$

The commercial FEM code known as ABAQUS was used to create the above mathematical FE model of a spherical vessel under internal–external pressure. A quarter of the sphere specimen geometry was addressed in the FEM model due to axisymmetric conditions. An 8-node biquadratic axisymmetric quadrilateral, reduced integration (CAX8R) element is used to represent the FGM sphere. 3050 elements in total, optimized from grid independent tests, were chosen for the final FEM model. Figure 2 shows the grid independent test for the FE model. A FORTRAN code USDFLD was written and then coupled with ABAQUS for capturing variations of nonlinear material properties along the radius.
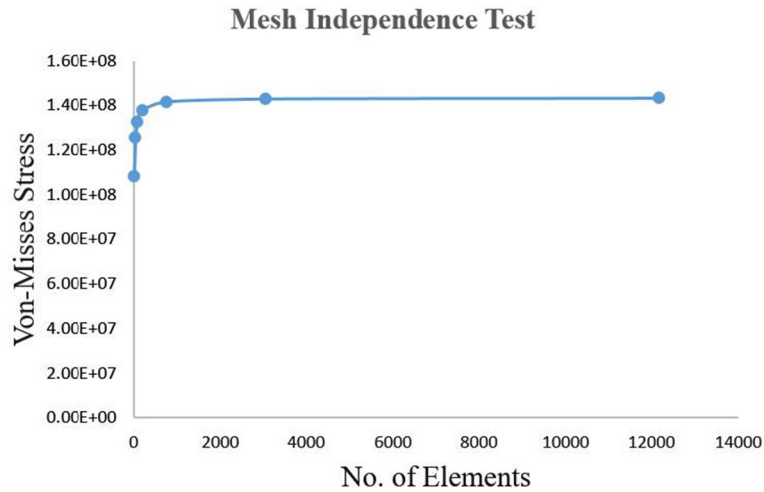
Fig. 2 Mesh independence test
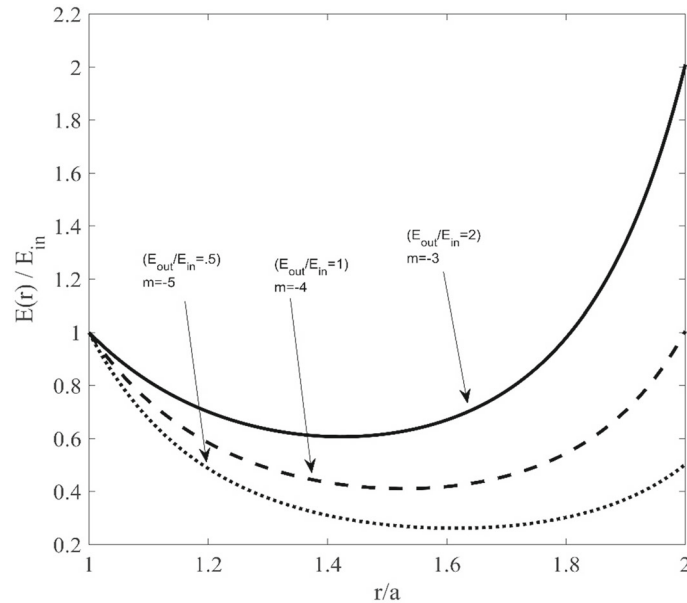
**Fig. 3** The variation of elastic modulus along the radial direction with various values of m

4 Results and discussions

Initially, a thick sphere with a varying radial modulus of elasticity is considered to illustrate the effectiveness of the present analysis. The inner and outer radii are $a = 0.1\,m$ and $b = 0.2\,m$ respectively. For convenience, it is assumed that Young modulus at the inner surface of the sphere $E_{in} = 200\,GPa$ and Poisson ratio $v = 0.3$. $P_{in} = 50, 250, 500$ MPa are the applied internal pressures, and in some cases, the outer is traction free ($P_{out} = 0$). The values of constants in Eq. (4) are changed to establish a condition for ease of analysis. The constants can be changed in a variety of ways to replicate these conditions. The values of $\gamma = 0.172$, and $s = 4.1$ according to [19]. The study was then carried out for variation of non-homogeneity parameters $m = -5, -4$, and -3, which correspond to the ratios $E_{out}/E_{in} = 0.5, 1$, and 2.

MAPLE program is written to carry out the analytical solution. In order to assess the efficiency and robustness of the present approach, the obtained analytical solution is compared with finite element method (FEM). The dimensionless Young modulus in the radial direction is presented in Fig. 3 for m $= -5, -4$, and -3, which correspond to the ratios $E_{out}/E_{in} = 0.5, 1$, and 2. According to this graph, the non-dimensional Yong modulus increases as m rises at the same radial location in $a < r < b$.
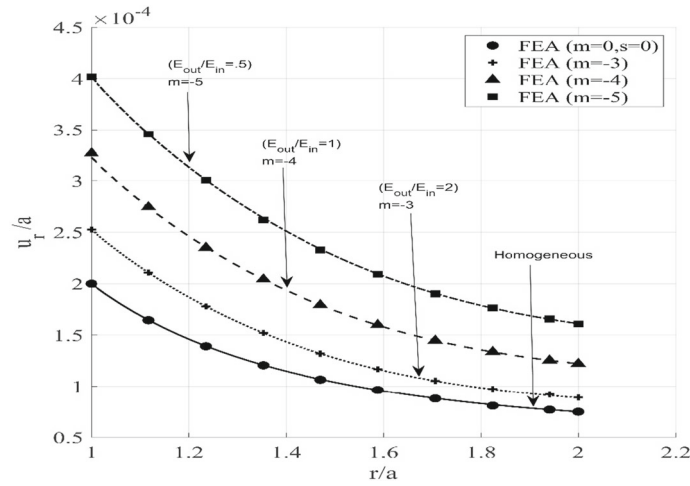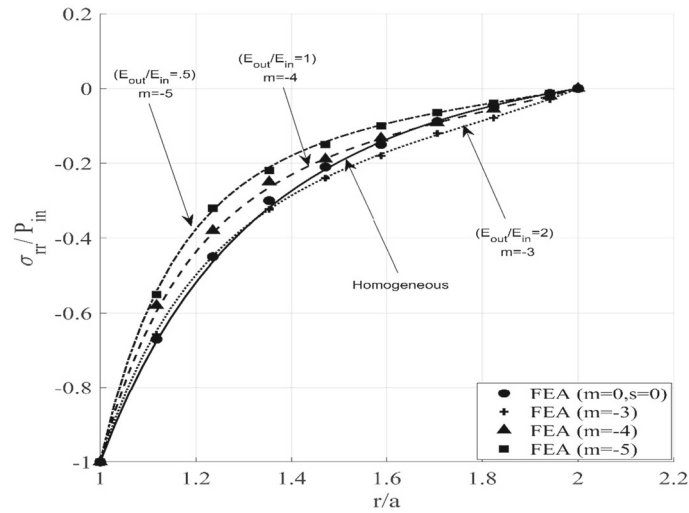
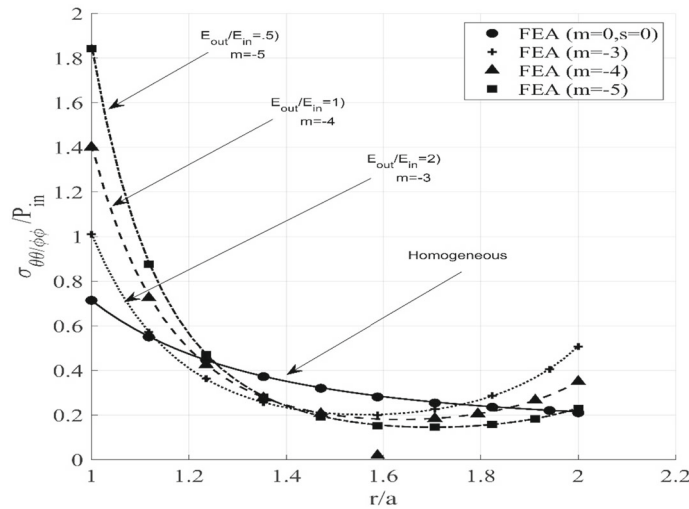**Fig. 4** The variation of normalized displacement along the radial direction for various values of *m*
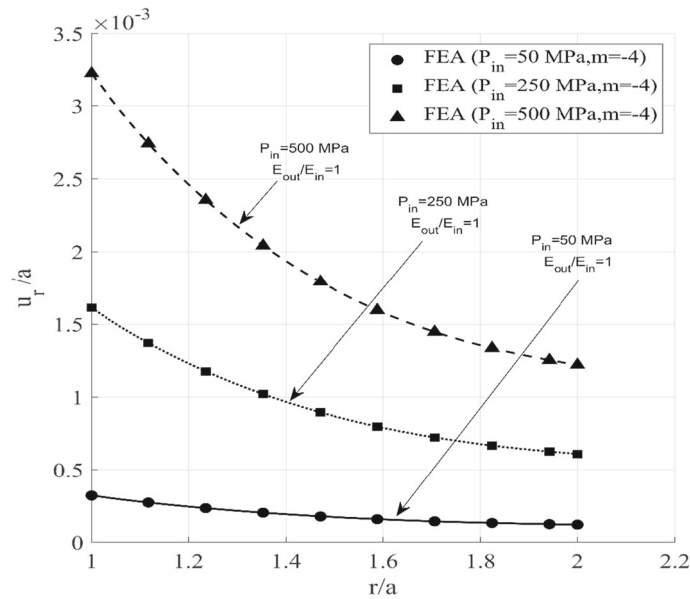
Fig. 5 The variation of normalized displacement along the radial direction for a particular value of $m = -4$, and changed values of interior pressure

It is noted that from Figs. 3 to 11, the continuous lines represent analytical results, whereas the discrete markers represent FEA results. The displacement fields obtained from FE and exact solutions along the radial direction of the sphere for various values of m are shown in Fig. 4. Figure 4 clearly demonstrates that radial displacements are greatest on the interior surface ($r = a$). From the inner surface to the outer surface, it is also seen that the radial displacement values steadily decrease. We get an increase in radial displacement with a decrease in *m*. The drop in *m* causes an increase in radial displacement because the sphere's global stiffness decreases. The displacement variation of heterogeneous materials is analogous to that of homogeneous materials. However, the displacements of the FGM spheres are larger than those of a regular sphere for the specified material inhomogeneity parameter.

Figure 5 depicts the fluctuation of the radial displacement resulting from FE and exact solutions along the radial direction of a sphere using a constant value of $m = -4$ and various values of interior pressure $P_i = 50, 250,$ and 500 MPa. The values of radial displacement decrease progressively from the inner to the outer surface but increase with increase in internal pressure.

Fig. 6 The variation of normalized stress along with the thickness for various values of m

Fig. 7 The variation of normalized circumferential stress along with the thickness for various values m

Figure 6 shows the normalized radial stress, as calculated by Eq. 12, for different values of $m = -5, -4,$ and -3. It is clearly shown that heterogeneous materials have a similar trend of radial stress variations compared to homogeneous materials. For all examined values of m, the stress along the radial direction increases monotonically with r. It was found that when m grows, the radial stress magnitude decreases for each fixed r in $a < r < b$. The reason behind this is that the sphere's overall rigidity increases. Equation 13's normalized circumferential stress was presented along the radial direction, as illustrated in Fig. 7. For all possible values of m, the hoop stress variation throughout the radius is similar to thick spheres composed of isotropic materials. This is because there is pressure acting within, yet there is no pressure acting externally. The value of hoop stress decreases as m grows in $r <\sim 1.5$ and converging in nature. However, when m grows, the tangential stress rises for each given value of r in $r >\sim 1.5$ m and diverges in nature.

The Von-Misses stress distribution obtained from Eq. 17 is plotted in the radial direction for the various values of m, as shown in Fig. 8. The equivalent stress variation is monotonous concerning r for all values of m. This pattern is comparable to the homogeneous FGM sphere. Misses stress increases on the inner surface with a reducing value of m, and decreases at the outer surface with increasing values of m. For all fixed values of r in r< ~1.2 m, the corresponding stress is shown to grow as m dropped. However, the corresponding stress grows as m rises for each fixed value of r in $r > \sim 1.2$ m. This is because an increase in the outer surface results in an increase in global stiffness.
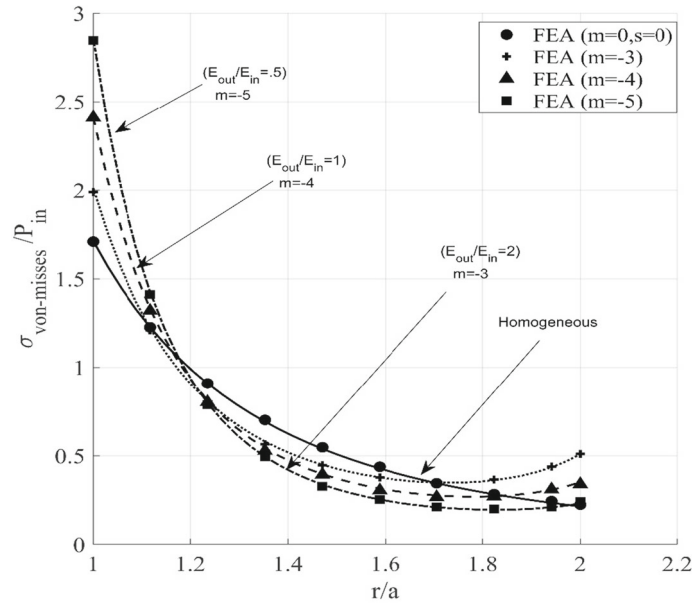
Fig. 8 The variation of Von-Misses stress along radial direction for various values of m
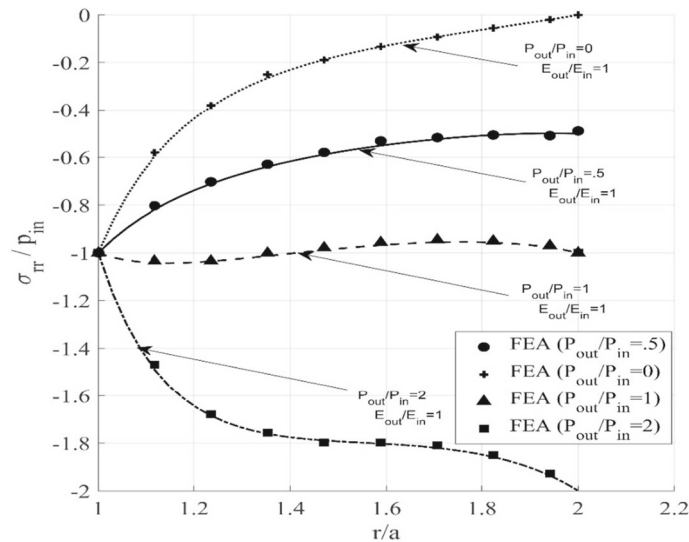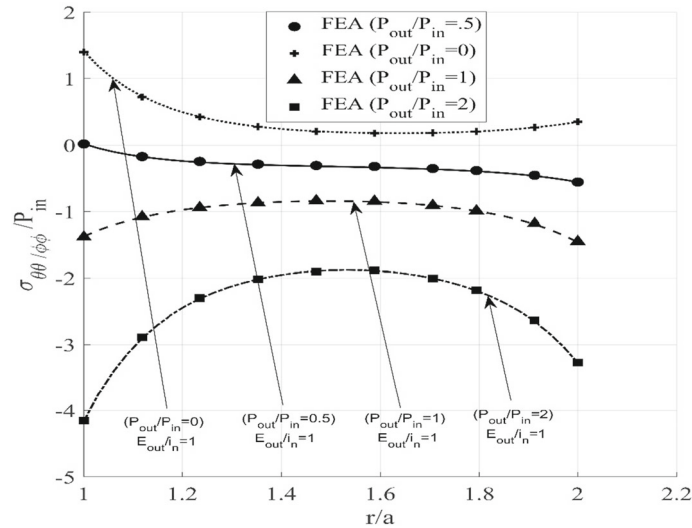

Fig. 9 The variation of normalized radial stress along with the thickness for a particular value of $m = -4$ and changed pressure ratios

Radial distribution for normalized radial stress for a fixed value of $m = -4$ and various pressure ratios such as $P_{out}/P_{in} = 0, 0.5, 1, 2$ are plotted in Fig. 9. Radial stress increases in nature for the pressure ratio $0 \leq P_{out}/P_{in} \leq .5$. Furthermore, its initial rate of increase is faster as material elasticity decreases. A slightly decreasing–increasing pattern is observed in the case of $P_{out}/P_{in} = 1$. In the case of $P_{out}/P_{in} = 2$, radial stress falls drastically in the region $1 \leq \frac{r}{a} \leq \sim 1.4$. After that, it remains invariant in the region of $1.4 \sim \leq \frac{r}{a} \leq \sim 1.5$, and then, it becomes decreasing in the left of the portion. Indeed, decreasing elasticity induced more compressive stress. Moreover, increasing the pressure ratio decreases the induced stress (tensile).

The radial distribution of normalized circumferential stress for a particular value of m and pressure ratios $P_{out}/P_{in} = 0, 0.5, 1, 2$ is plotted in Fig. 10. In the case of $P_{out}/P_{in} = 0$; it can be shown that as elasticity reduces, produced circumferential stress drops as well, after which it stays invariant. The induced stress becomes almost constant in the case of $P_{out}/P_{in} = 0.5$. The stress trend line for the scenario $1 \leq (P_{out}/P_{in}) = 0 \leq 2$ is the reverse of the instance $P_{out}/P_{in} = 0$. The circumferential stress rises and then falls in case $1 \leq$

Fig. 10 The variation of normalized circumferential stress for a particular value of $m = -4$ and changed pressure ratios

$(P_{out}/P_{in}) = 0 \leq 2$, making a dome shape. Furthermore, the higher the pressure ratio dome shape becomes more concave. It is because elastic modulus falls in the middle region of the sphere; that is why maximum stress is found at the central layers.

The distribution of normalized Von-Misses stress for a certain value of $m = -4$ and different pressure ratios are plotted in Fig. 11. The equivalent stress appears to be symmetric about $r/a = 1.5$ for $P_{out}/P_{in} = 1$. It is observed that from $r/a = 0$ to $r/a = 1.5$, the stress value initially decreases, then after a certain value, it increases, and the left of the portion is reflected. For instance $P_{out}/P_{in} = 0.5$, the diminishing character of equivalent stress is discovered. When $P_{out}/P_{in} = 2$, however, Von-Misses stress falls for each value of r in $/a \leq\sim 1.5$, whereas it rises for each particular value of r in $r/a \geq\sim 1.5$ m. In the case of $P_{out}/P_{in} = 0$, an increasing–decreasing pattern of equivalent stress is noticed, similar to $P_{out}/P_{in} = 2$. In addition to the above analytical and numerical results, stress and displacement fields for mechanical loading are also presented. Figure 12 shows the radial displacements, radial stresses, circumferential stresses, and failure stresses values that are obtained from FEA (ABAQUS) results. It is evident from the contour plot (Fig. 12) of FEA data that the displacement of the inner surface (12a) of the sphere is higher than the outer surface. On the other hand, the radial stress on the inner surface is less than the sphere's outer surface (12c). However, Von-Misses and Hoop follow the same nature (Fig. 12b and d). Finally, it can be mentioned that the contour plots and the graphical data (Figs. 3 to 11) have a good agreement.

5 Conclusions

An analytical formulation was offered in this study to determine the displacements and stress fields in a thick-walled sphere that was under interior as well as exterior pressure. A nonlinear equation with four parameters along the sphere's thickness was projected to describe the change in FGM properties. The acquired outcomes were compared to those of an isotropic sphere. For different pressures and varying material inhomogeneity parameters, the findings are represented as the evolution of various stress fields along the radial direction. Based on the findings presented above, we draw the conclusion that the spatial variation in material stiffness has a significant impact on the distribution of stresses as well as displacement fields in the FGM Sphere. Therefore, the non-homogeneous parameter is a helpful tool from the standpoint of design; it may be adapted to various applications in order to regulate the stress fields. For the purpose of validation, the FE model of the sphere under pressure was created. Within this model, a FE code was utilized to accomplish the continuous changing of the Young modulus along with the radial directions. Furthermore, the analytical and numerical solutions were then contrasted with one another. The validity of the analytical model was demonstrated by the fact that there was a high degree of similarity between the numerical findings and the exact solutions. When an analytical approach fails to provide a solution or is too time-consuming, the FE solutions might be
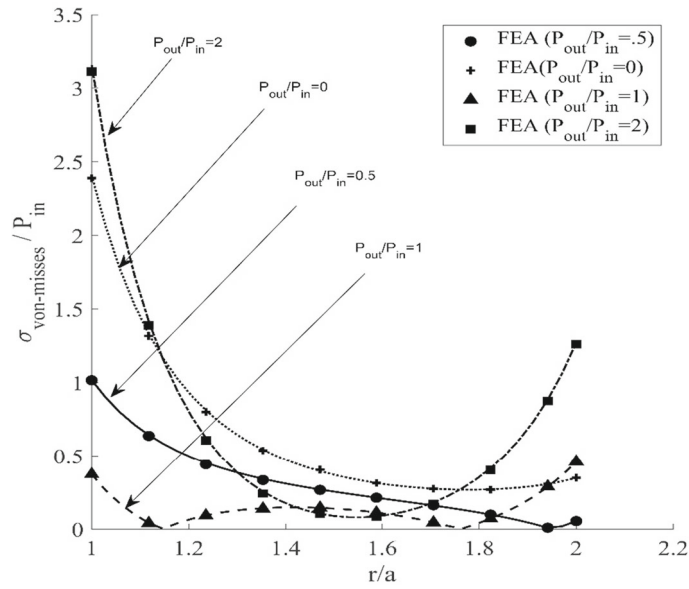
Fig. 11 The variation of normalized Von-Misses stress for a particular value of $m = -4$ and changed pressure ratios
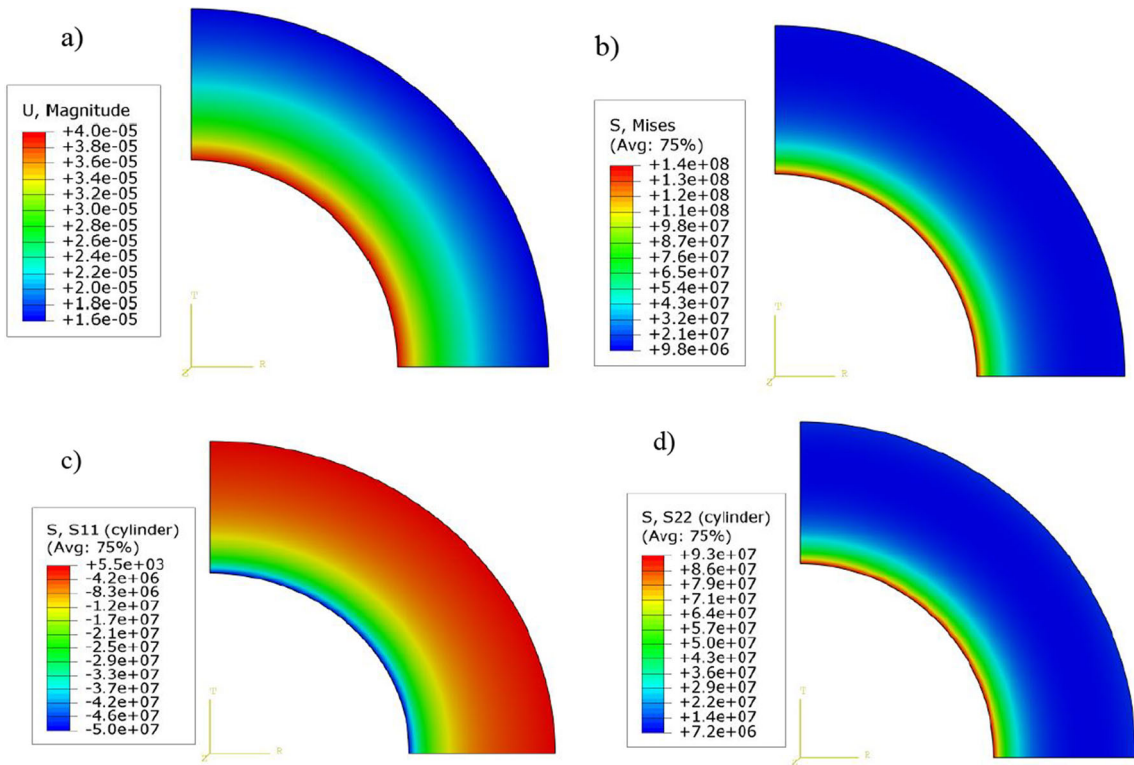

Fig. 12 Stress and displacement fields obtained using the ABAQUS code, with **a** radial displacement; **b** failure stress; **c** radial stress distribution; and **d** hoop stress distribution

useful to solve much more complicated problems, optimize parameters, and create a novel FGM according to customized preferences.

Declarations

Conflict of interest We would like to confirm that there is no known conflict of interests associated with this publication, and there has been no significant financial support for this work that could have influenced its outcome.

References

1. Benslimane, A., Bouzidi, S., Methia, M.: Displacements and stresses in pressurized thick-walled FGM cylinders: exact and numerical solutions. Int. J. Press. Vessel. Pip. **168**, 219–224 (2018)
2. Sharma, D., Kaur, R.: Thermoelastic analysis of FGM hollow cylinder for variable parameters and temperature distributions using FEM. Nonlinear Eng. **9**, 256–264 (2020)
3. Benslimane, A., Benchallal, R., Mammeri, S., Methia, M., Khadimallah, M.A.: Investigation of displacements and stresses in thick-walled FGM cylinder subjected to thermo-mechanical loadings. Int. J. Comput. Methods Eng. Sci. Mech. **22**, 138–149 (2020)
4. Kiani, Y., Eslami, M.R.: The GDQ approach to thermally nonlinear generalized thermoelasticity of a hollow sphere. Int. J. Mech. Sci. **118**, 195–204 (2016)
5. Farhan, A.M., Abd-Alla, A.M., Khder, M.A.: Solution of a problem of thermal stresses in a non-homogeneous thermoelastic infinite medium of isotropic material by finite difference method. J. Ocean Eng. Sci. **4**, 256–262 (2019)
6. Celebi, K., Yarimpabuç, D., Keles, I.: A novel approach to thermal and mechanical stresses in a FGM cylinder with exponentially-varying properties. J. Theor. Appl. Mech. **55**, 343–351 (2017)
7. Bahoum, K., Diany, M., Mabrouki, M.: Stress analysis of compound cylinders subjected to thermo-mechanical loads. J. Mech. Sci. Technol. **31**, 1805–1811 (2017)
8. Das, P., Islam, M.A., Somadder, S., Hasib, M.A.: Analytical and numerical analysis of functionally graded (FGM) axisymmetric cylinders under thermo-mechanical loadings. Mater. Today Commun. **33**, 104405 (2022)
9. Tutuncu, N., Ozturk, M.: Exact solutions for stresses in functionally graded pressure vessels. Compos. Part B Eng. **32**, 683–686 (2001)
10. You, L.H., Zhang, J.J., You, X.Y.: Elastic analysis of internally pressurized thick-walled spherical pressure vessels of functionally graded materials. Int. J. Press. Vessel. Pip. **82**, 347–354 (2005)
11. Eslami, M.R., Babaei, M.H., Poultangari, R.: Thermal and mechanical stresses in a functionally graded thick sphere. Int. J. Press. Vessel. Pip. **82**, 522–527 (2005)
12. Poultangari, R., Jabbari, M., Eslami, M.R.: Functionally graded hollow spheres under non-axisymmetric thermo-mechanical loads. Int. J. Press. Vessel. Pip. **85**, 295–305 (2008)
13. Chen, Y.Z., Lin, X.Y.: Elastic analysis for thick cylinders and spherical pressure vessels made of functionally graded materials. Comput. Mater. Sci. **44**, 581–587 (2008)
14. Tutuncu, N., Temel, B.: A novel approach to stress analysis of pressurized FGM cylinders, disks and spheres. Compos. Struct. **91**, 385–390 (2009)
15. Borisov, A.V.: Elastic analysis of multilayered thick-walled spheres under external load. Mechanics. **84**, 28–32 (2010)
16. Sadeghian, M., Toussi, H.E.: Axisymmetric yielding of functionally graded spherical vessel under thermo-mechanical loading. Comput. Mater. Sci. **50**, 975–981 (2011)
17. Nejad, M.Z., Abedi, M., Lotfian, M.H., Ghannad, M.: An exact solution for stresses and displacements of pressurized FGM thick-walled spherical shells with exponential-varying properties. J. Mech. Sci. Technol. **26**, 4081–4087 (2012)
18. Karami, K., Abedi, M., Zamani Nejad, M., Lotfian, M.H.: Elastic analysis of heterogeneous thick-walled spherical pressure vessels with parabolic varying properties. Front. Mech. Eng. **7**, 433–438 (2012)
19. Atashipour, S.A., Sburlati, R., Atashipour, S.R.: Elastic analysis of thick-walled pressurized spherical vessels coated with functionally graded materials. Meccanica **49**, 2965–2978 (2014). https://doi.org/10.1007/s11012-014-0047-2
20. Dryden, J., Jayaraman, K.: Effect of inhomogeneity on the stress in pipes. J. Elast. **83**, 179–189 (2006)
21. Bell, W.W.: Special functions for scientists and engineers. Courier Corporation, USA (2004)
22. Abramowitz, M., Stegun, I.A., Romer, R.H.: Handbook of mathematical functions with formulas, graphs, and mathematical tables. Am. J. Phys. **56**, 958 (1988)